Scripta Materialia 199 (2021) 113861

Contents lists available at ScienceDirect

Scripta Materialia

journal homepage: www.elsevier.com/locate/scriptamat

Critical crystallization properties of an industrial-grade Zr-based metallic glass used in additive manufacturing

Navid Sohrabi[a,*], Jürgen E.K. Schawe[b,c], Jamasp Jhabvala[a], Jörg F. Löffler[b], Roland E. Logé[a]

[a] Thermomechanical Metallurgy Laboratory (LMTM), PX Group Chair, Ecole Polytechnique Fédérale de Lausanne (EPFL), 2002 Neuchâtel, Switzerland
[b] Laboratory of Metal Physics and Technology, Department of Materials, ETH Zurich, 8093 Zurich, Switzerland
[c] Mettler-Toledo GmbH, Analytical, 8606 Nänikon, Switzerland

ARTICLE INFO

Article history:
Received 15 January 2021
Revised 25 February 2021
Accepted 5 March 2021
Available online 17 March 2021

Keywords:
Metallic glass
Crystallization
Fast differential scanning calorimetry
Laser powder-bed fusion
Additive manufacturing

ABSTRACT

The major challenge to overcome when processing metallic glasses (MGs) is to avoid crystallization. Therefore, time-temperature-transformation (TTT) diagrams are used, but they are often derived from experiments in which heating or cooling rates are limited and do not cover the full range of processing conditions, especially those encountered in additive manufacturing (AM) where the rates are very high. Here, an industrial-grade Zr-based MG (AMZ4) is investigated via fast differential scanning calorimetry (FDSC). The critical cooling and heating rates of AMZ4 are experimentally measured and TTT diagrams are determined upon heating and cooling. The critical heating rate of 45,000 K/s is 18 times the critical cooling rate, which indicates the presence of a self-doped glass (SDG) that includes quenched-in nuclei. The results illustrate that AMZ4 is very sensitive to crystallization, even in laser-based AM conditions, where heating and cooling steps need to be distinguished.

Metallic Glasses (MGs) refer to alloys that have the ability to solidify in the amorphous state upon cooling from the melt provided that the cooling rate is high enough [1]. AMZ4 is one of the Zr-based MGs free of Be and Ni. It has been designed in the last decade and is composed of Zr, Cu, Al, and Nb ($Zr_{59.3}Cu_{28.8}Al_{10.4}Nb_{1.5}$, in at.%) [2].

The cost is one of the main criteria for the selection of an alloy for industrial applications. Industrial-grade alloys are often less expensive, but they contain more impurities, such as oxygen [3]. The adverse effect of oxygen content on the glass-forming ability and thermal stability of Zr-based bulk MGs (BMGs) has been previously studied [4,5].

Industrial-grade AMZ4 powder has recently gained great attention in laser-based additive manufacturing (AM) methods, such as laser powder-bed fusion (LPBF) [6–11]. Customized design, low waste, the possibility of producing complex geometry and larger size fabrication have made LPBF a prominent candidate compared to other conventional processing methods such as casting [12].

Since the interaction time between the laser and the deposited powder is short and confined to a small volume the local cooling rate (β_c) can reach 10^3 to10^8 K/s [13], which is typically higher than the critical cooling rate ($\beta_c{}^c$) of most MGs [1,14,15]. Several BMGs based on Al [16], Cu [17], Fe [18], Ti [19], Zr [6–11,20–23], and Pd [24] have been fabricated via LPBF.

Although the mentioned processing techniques induce high cooling rates, crystallization of industrial-grade AMZ4 has been reported in several studies [6–11,21]. According to Liu et al. [25], crystallization in AM-produced Zr-based ($Zr_{65}Cu_{15}Ni_{10}Al_{10}$) BMG parts occurs upon reheating the solidified material during laser processing due to the adding of new layers. Yang et al. [22] and Ouyang et al. [23] investigated LPBF of a $Zr_{55}Cu_{30}Ni_5Al_{10}$ BMG and underlined the time spent above the crystallization temperature (a few milliseconds) in the heat-affected zone (HAZ) of the melt pool as crucial for the crystallization process. However, the crystallization temperature was measured by conventional differential scanning calorimetry (DSC) at a heating rate of 20 K/min, which is far below the heating and cooling rates experienced in the LPBF process. It is well established that an increase in the heating rate significantly influences glass transition and crystallization temperatures [10]. Therefore, to unravel the reason behind crystallization, a characterization technique considering higher heating and cooling rates is required.

Fast differential scanning calorimetry (FDSC) has made possible detailed studies of structure formation at heating rates (β_h) and cooling rates (β_c) of up to more than 10^4 K/s [26]. This technique

* Corresponding author.
E-mail address: navid.sohrabi@epfl.ch (N. Sohrabi).

https://doi.org/10.1016/j.scriptamat.2021.113861

has been extensively used to study crystallization in various MG alloys [27–34]. Ericsson et al. [21] prepared a TTT diagram upon cooling for AMZ4 by FDSC and also used it for a numerical simulation of the LPBF process. However, a corresponding TTT diagram upon heating, and continuous heating and cooling transformation (CHT and CCT) diagrams, would describe more realistically the AM process. In our previous study [10], using numerical simulations we estimated that the heating and cooling rates of LPBF on AMZ4 were 1×10^6 K/s and 5×10^5 K/s, respectively. Despite these high rates nanocrystals were detected in the HAZ. The origin of the crystallization behavior at such high rates of temperature changes needs to be better understood.

Despite the great interest in the application of AMZ4, knowledge on the solidification process and crystallization of this material is still limited and the few reported data differ significantly from one another [2,6,21,35–37]. However, such data are important in order to adjust the processing parameters to increase the relatively low thermal stability, which is one of the main technological problems during the processing of this material.

In this work, the critical cooling and heating rates ($\beta_c{}^c$ and $\beta_h{}^c$) of industrial-grade AMZ4 have been measured by FDSC and time-temperature-transformation (TTT) diagrams upon heating and cooling, and continuous heating and cooling transformation (CHT and CCT) diagrams, have been experimentally constructed. The results of the present study can thus be used e.g. for finite element simulations of AM or casting processes to predict crystallization and describe the related processing conditions.

Pre-alloyed gas-atomized amorphous AMZ4 powder (with an oxygen content of around 1300 ppm [10]), supplied by Heraeus Additive Manufacturing GmbH, with a nominal chemical composition of $Zr_{59.3}Cu_{28.8}Al_{10.4}Nb_{1.5}$ was used for the FDSC experiments. The measurements were performed using a Flash DSC 2+ (Mettler-Toledo) with a UFH-1 sensor and equipped with an HC100 intracooler (Huber); for details see Refs. [26,38]. To reduce the oxygen content of the purge gas, the sensor support was sealed with a screw-on lid, and argon (99.999% purity) with a flow rate of 80 ml/min was used. The temperature of the sensor support was set to −40 °C. The preparation step for the sensor (denoted as "correction") was performed at the same conditions. For sample positioning, the active zone on the sample side of the sensor was wetted with a thin film of silicon oil (AK 60000 from Wacker Chemie). Before the first measurement, the sample was purged for 45 min. The oil evaporates and decomposes during the first heating.

In prior experiments, it was found that the crystallization kinetics of individual powder particles shows large variations of the critical heating rate with values between 30,000 and more than 60,000 K/s. This may be due to the influence of sample size on the crystallization kinetics, which occurs for samples below a critical size [28]. Therefore, the sample size was varied to find the optimum experimental conditions. Fluctuations are significantly reduced (to between 40,000 and 50,000 K/s) in samples containing three to five particles, with a typical overall mass of 0.3 μg. The particles were molten together on the sensor in such a way that they form a single particle, as a collection of individual particles usually leads to multiple crystallization events.

To measure the cooling-rate dependence of crystallization, samples were cooled with rates between 200 K/s and 40,000 K/s from the liquid state, and subsequently heated at 5000 K/s. The time-temperature curves are shown as inset in Fig. 1a. The glass transition occurs above 400 °C and crystallization occurs between 650 °C and 800 °C, followed by a complex melting range. The intensity of the glass transition (ΔC_p) and the enthalpy of crystallization (ΔH_c) are plotted against the cooling rate in Fig. 1b. We evaluated both events simultaneously to have an additional indication that the sample was previously amorphous after fast cooling and that the exothermal peak can be interpreted as a crystallization process. At cooling with relatively low rates (200 K/s $\leq \beta_c <$ 800 K/s) the sample crystallizes completely. Thus, no glass transition and crystallization occur during heating. After cooling between 800 K/s and 2500 K/s, the glass transition intensity and the crystallization enthalpy increase with increasing cooling rate. This is the cooling-rate range that leads to a semi-crystalline glass, i.e. a MG composite that consists of a glassy and crystalline phase. When cooling at higher rates ($\beta_c >$ 2500 K/s), the sample does not crystallize anymore, and ΔH_c and ΔC_p remain constant. Consequently, the critical cooling rate is determined to be 2500 K/s. In our previous work [10], using finite element (FE) simulations, we calculated β_c in the melt pool of the LPBF process as 5×10^5 K/s, which is two orders of magnitude faster than the $\beta_c{}^c$ of AMZ4. Therefore, in the LPBF process the initial cooling cycle from the melt should not lead to crystallization of AMZ4.

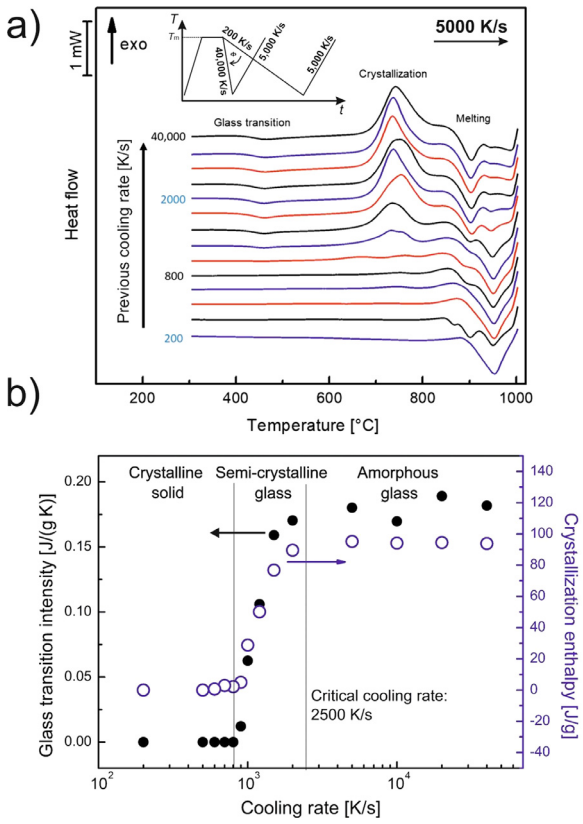

Fig. 1. (a) FDSC scan of AMZ4 measured with 5000 K/s heating rate after cooling at different rates (β_c) from 200 K/s to 40,000 K/s (the inset illustrates the applied temperature-time program). (b) Intensity of the glass transition and enthalpy of crystallization of AMZ4 during heating as a function of the previous cooling rate (log scale). Three regions corresponding to a crystalline solid, a semi-crystalline glass and an amorphous glass can be distinguished.

The FDSC curves in Fig. 1a show a complex melting process with two main peaks at approximately 905 and 950 °C. In the case where the sample is completely crystallized during cooling ($\beta_c \leq$ 800 K/s), the main melting peak is at 950 °C. After cooling at rates larger than $\beta_c{}^c =$ 2500 K/s, it is at 905 °C. The difference in melting temperatures indicates the appearance of two different crystalline phases that form during slow cooling or heating of the glass [39].

To determine the critical heating rate, AMZ4 was heated at different rates between 1000 and 60,000 K/s (Fig. 2a). As illustrated in the inset for the temperature-time program, after achieving a stable liquid the sample was cooled with a β_c of 10,000 K/s, which is four times the critical cooling rate, to ensure that a glass has formed after cooling. The curves in Fig. 2a indicate that the

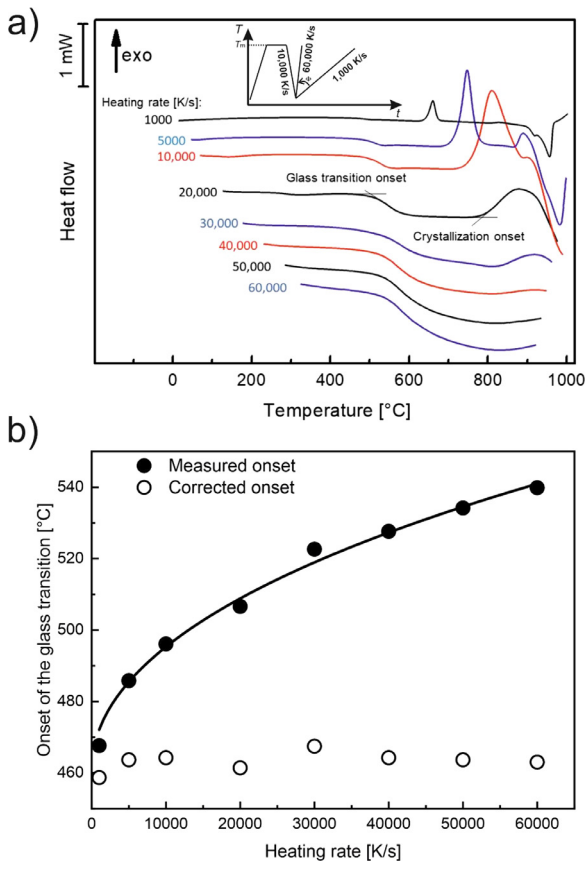

Fig. 2. (a) FDSC curves of AMZ4 measured at different heating rates (β_h) between 1000 K/s and 60,000 K/s after cooling the melt at a rate of 10,000 K/s (the inset illustrates the applied temperature-time program). (b) Measured onset of the glass transition versus heating rate (solid dots) and fit according to eq. (2); the open dots are the corrected onset temperatures.

measured onset temperatures for the glass transition and crystallization increase and that the crystallization enthalpy decreases with increasing heating rate. When heating with $\beta_h > 40{,}000$ K/s, no crystallization occurs. Thus, the critical heating rate of AMZ4 to bypass crystallization is determined to be $\beta_h{}^c \approx 45{,}000$ K/s. The comparison of the critical scanning rates shows that $\beta_c{}^c = 2500$ K/s $\ll \beta_h{}^c$, which reveals that a self-doped glass (SDG) comprising quenched-in nuclei has formed (for more details, see Ref. [40]). The numerically computed heating and cooling rates of AMZ4 in the LPBF process are 1×10^6 K/s and 5×10^5 K/s [10], respectively, and thus much higher than the critical values measured here. Nevertheless, crystallization has been detected in [10], illustrating that (constant) critical heating and cooling rates are not enough to describe the AMZ4 crystallization behavior in the LPBF process. This has also been demonstrated in [32], where BMG casting was monitored by high-speed infrared experiments and complementary FDSC studies.

To determine the real onset temperature of crystallization, the measured onset temperature has to be corrected considering the influence of heat-transfer conditions in the calorimeter. The simplest correction considers the thermal lag (τ), where the measured onset temperature of a thermal event ($T_{on,m}$) is described by [41]:

$$T_{on} = T_{on,m} - \tau\beta, \tag{1}$$

where T_{on} is the real onset temperature of the thermal event and β is the scanning rate.

Usually τ is rate independent. Using small samples and high heating rates, the linear approach of eq. (1) may, however, be violated. In such a case, the measured onset temperature is better described by a phenomenological equation [42]:

$$T_{on,m} = T_{on} + a\beta + b\beta^{0.5}, \tag{2}$$

where a and b are constants. The heating-rate dependent apparent thermal lag is then:

$$\tau(\beta) = a + b\beta^{-0.5}. \tag{3}$$

The parameters for the temperature correction are usually determined by the use of calibration materials (pure metals). For FDSC, the temperature corrections depend strongly on the heat contact between the sensor and the sample and the heat-transfer conditions in the sample [43]. Consequently, the thermal lag should be determined directly from the sample under investigation. Because of the complex melting behavior of AMZ4 the use of the melting-peak onset is not straightforward, but another option is the glass transition. If the glass transition temperature (T_g) is determined as a limiting fictive temperature [44,45], the T_g of an non-annealed sample and the width of the transformation depend only on the cooling rate but are independent of the heating rate [46,47]. In the heating-rate range used the apparent heating-rate dependence of non-annealed glasses is thus caused by thermal lag. The heat-flow curves in Fig. 2a are measured after previous cooling at a rate of 10,000 K/s. The thermal lag is then determined from the onset temperature of T_g (Fig. 2b). The solid curve in Fig. 2b is the fit result of Eq. (2) to the measured values, with the parameters $T_{on} = 461.0$ °C, $a = -1.15 \times 10^{-4}$ s and $b = 0.35$ (K.s)$^{0.5}$. The resulting corrected onsets of T_g are independent of the heating rate and approximately 465 °C. Comparison with the use of the heating-rate dependent melting temperatures of Pb and In to correct for thermal lag revealed that the uncertainties at high heating rates are larger than with the presented method.

The corrected onset temperatures of the crystallization peaks upon heating and cooling have been determined from Eq. (1) and are plotted in Fig. 3a as a function of the scanning rate. This diagram indicates also the critical cooling and heating rates.

The TTT diagrams of AMZ4 measured upon heating and cooling are presented in Fig. 3b. To obtain the TTT diagram upon heating, the sample was cooled from the melt with a rate of 20,000 K/s (eight times $\beta_c{}^c$) to far below the glass transition temperature, and subsequently heated with a rate of 50,000 K/s (faster than $\beta_h{}^c$) to the crystallization temperature (T_x). During an isothermal segment at T_x, a crystallization peak appears. The times of the onset, peak, and end-set were determined and plotted in Fig. 3b. In the region of maximum crystallization rate, the data scatter significantly (at a logarithmic scale), which is due to the stochastics of nucleation near the nose of the TTT diagram [40] and, in the present case, the experimental uncertainty of measuring such small onset times close to the time resolution of the sensor. The TTT diagram upon cooling is determined in a similar way. Samples were cooled directly from the melt with 20,000 K/s to T_x. Usually, the maximum rate of nucleation occurs at temperatures lower than the maximum rate of growth [48]. Consequently, by heating from the glassy state a self-doped glass [40] includes more nuclei before isothermal crystallization than a sample that is quenched from the melt. Therefore, the TTT diagram upon heating is shifted to shorter times compared to the one upon cooling, which has also been observed for other MGs [29]. The lack of nuclei at high temperatures upon cooling from the melt (due to a low nucleation rate) explains the missing data points in the TTT curve upon cooling. This TTT curve is bimodal, with a maximum crystallization rate (nose) at about 750 °C and a second one at 640 °C. Thus, different kinds of nuclei might form at these relatively low temperatures. The peak time at the upper nose of the TTT curve upon cooling is around 35 ms, which is longer than that measured in Ref. [21]. This discrepancy may be attributed to the fact that in

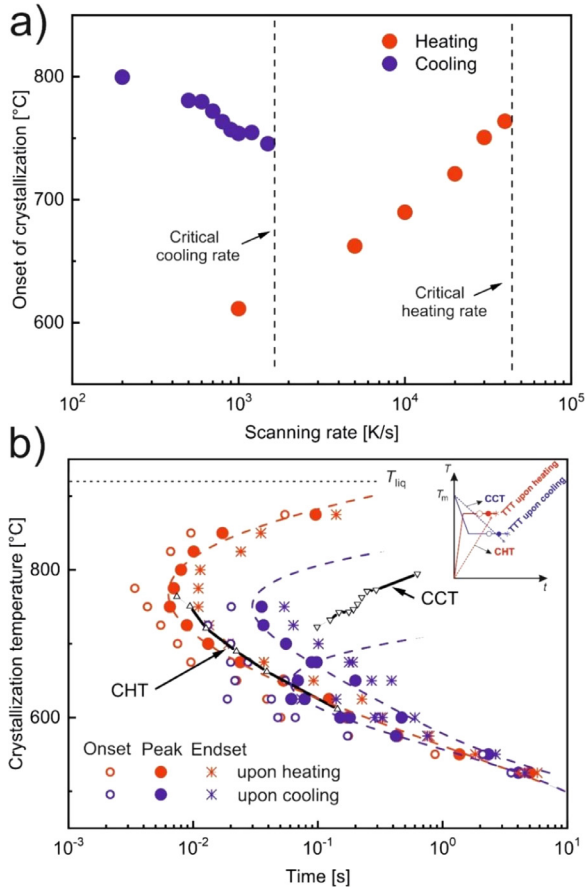

Fig. 3. (a) Corrected onset temperatures of the crystallization peaks measured upon heating and cooling. The dashed lines indicate the critical scanning rates above which no crystallization occurs. (b) Isothermal TTT-diagrams of AMZ4 measured upon heating from the amorphous state and cooling from the melt; shown are values for the onset, maximum, and end-set of the crystallization peaks. The dashed curves are guides to the eyes for the peak maxima. The solid lines with small triangles are the CHT and CCT curves. The inset illustrates how these curves were measured.

Ref. [21] only a single powder particle was used, generating a high uncertainty in the measurement, and that no oxygen content was specified.

The CHT diagram is also displayed in Fig. 3b. The temperature is the corrected onset temperature of the primary crystallization peak upon heating (Fig. 3a). The corresponding time is the difference between the corrected crystallization onset and the glass transition onset divided by the heating rate. This curve fits well with the low-temperature side of the TTT diagram upon heating, but is shifted slightly to the right. This may be due to the fact that crystallization during heating starts already before the peak onset. The real start of crystallization cannot be detected in the heating curve due to its slow initial rate during heating [49].

The CCT diagram is obtained from the corrected crystallization onset temperature upon cooling versus the dwell time in the temperature range of possible crystallization. This time is the difference between the liquidus temperature (T_{liq} = 919 °C [5]) and the corrected crystallization onset (Fig. 3a) divided by the cooling rate. The CCT curve appears at slightly lower temperatures than the extrapolation of the TTT curve in Fig. 3b (dashed blue curve above 750 °C for the upper TTT diagram upon cooling). The sample dwells apparently a relatively long time in the high-temperature region, with very low probability of nucleation.

The TTT diagrams and the CHT and CCT curves are useful in understanding the isothermal and isochronal crystallization behaviors of AMZ4. The time to crystallization is very short and limits the processing methods for the fabrication of bulk amorphous AMZ4. The reason for such short times to crystallization may be related to the relatively high amount of oxygen content in the industrial-grade AMZ4 [6]. As mentioned earlier, the HAZ of the melt pool in laser-based AM methods experiences reheating (not exceeding the melting point). If the thermal history of different locations in the HAZ is superimposed on the TTT and CHT diagrams, some locations in the HAZ are expected to intersect with the diagrams. This signifies that those locations experience high temperatures for a sufficient amount of time to form (nano-)crystals [10]. The diagrams may also explain why crystallization could not be avoided in AMZ4 samples fabricated by casting [35] and spark plasma sintering [37].

It is well established that crystallization in AM of metallic glasses happens during the thermal cycles generated by the successive addition of layers, which undergo each time locally fast melting and solidification with varying heating and cooling rates. Crystallization occurs in the heat-affected zones of the melt pools, i.e. in the zones which remain solid at temperatures close to the melting point [10]. Optimizing the laser parameters thus consists of making sure that the heating and cooling parts of the thermal cycles minimize crystallization. To map such processes by measurements, it is important to measure or extrapolate to the required rates of temperature change. The FDSC technology makes this possible and representative samples can be obtained by selecting a proper sample size to minimize size-dependent effects. The measured crystallization behavior of AMZ4 by FDSC also enables the description of the solidification behavior at very short time scales.

In AM technology the processing parameters can be easily tuned to prevent a too high temperature in the melt pool and thus to avoid an excessive increase of the part's average temperature. The crystallization behavior at very short time scales in regions close to melt pool is, however, much more difficult to control and predict. In this context, FDSC data provide critical information for the general improvement of AM processes .

In this study, calorimetric investigations of an industrial-grade Zr-based metallic glass (AMZ4) have been performed using FDSC. It was shown that FDSC is a suitable characterization method to study the crystallization behavior of metallic glasses with low thermal stability. A semi-crystalline glass formed during cooling with a rate between 800 K/s and 2500 K/s. The critical cooling and heating rates of the alloy were determined as 2500 K/s and 45,000 K/s, respectively. This large difference indicates that a self-doped glass (SDG) with quenched-in nuclei formed during cooling. As chemically homogeneous glasses (CHGs) do not contain quenched-in nuclei [40], the use of materials that form CHGs would be preferred in AM processes. Differences in the melting temperature during slow and fast heating and cooling, respectively, illustrate the formation of two different crystalline structures. The time to the peak of crystallization upon heating is almost one order of magnitude shorter than upon cooling. The TTT, CHT, and CCT diagrams measured in this study reveal that AMZ4's time to crystallization is short and that the alloy's thermal stability is low. This makes the production of bulk glassy parts by methods such as casting, sintering, and laser-based additive manufacturing very challenging. Understanding the crystallization behavior of this alloy can, however, help predicting the final structure, based on the estimated heating and cooling rates and the time spent at high temperature induced by the chosen processing method.

This work was supported by the "PREcision Additive Manufacturing of Precious metals Alloys (PREAMPA)" project, funded by the Swiss ETH domain within the Strategic Focus Area on Advanced Manufacturing. The generous support of PX Group to the LMTM laboratory is also gratefully acknowledged.

Declaration of Competing Interest

The authors declare that they have no known competing financial interests or personal relationships that could have appeared to influence the work reported in this paper.

References

[1] J.F. Löffler, Intermetallics 11 (2003) 529–540.
[2] J. Heinrich, R. Busch, B. Nonnenmacher, Intermetallics 25 (2012) 1–4.
[3] D.V. Louzguine-Luzgin, C. Suryanarayana, T. Saito, Q. Zhang, N. Chen, J. Saida, A. Inoue, Intermetallics 18 (2010) 1531–1536.
[4] X.H. Lin, W.L. Johnson, W.K. Rhim, Mater. Trans. JIM 38 (1997) 473–477.
[5] I. Jonas, W. Hembree, F. Yang, R. Busch, A. Meyer, Appl. Phys. Lett. 112 (2018) 1–5.
[6] V. Pacheco, D. Karlsson, J.J. Marattukalam, M. Stolpe, B. Hjörvarsson, U. Jansson, M. Sahlberg, J. Alloys Compd. 825 (2020) 153995.
[7] J.J. Marattukalam, V. Pacheco, D. Karlsson, L. Riekehr, J. Lindwall, F. Forsberg, U. Jansson, M. Sahlberg, B. Hjörvarsson, Addit. Manuf. 33 (2020) 101124.
[8] W. Tillmann, A. Fehr, J. Wegner, D. Stangier, S. Kleszczynski, G. Witt, Surf. Coatings Technol. 386 (2020) 125463.
[9] J. Lindwall, V. Pacheco, M. Sahlberg, A. Lundbäck, L.E. Lindgren, Addit. Manuf. 27 (2019) 345–352.
[10] N. Sohrabi, J. Jhabvala, G. Kurtuldu, M. Stoica, A. Parrilli, S. Berns, E. Polatidis, S. Van Petegem, S. Hugon, A. Neels, J.F. Löffler, R.E. Logé, Mater. Des. 199 (2021) 109400, doi:10.1016/j.matdes.2020.109400.
[11] N. Sohrabi, R.S. Panikar, J. Jhabvala, A.R. Buch, S. Mischler, R.E. Logé, Surf. Coatings Technol. 400 (2020), doi:10.1016/j.surfcoat.2020.126223.
[12] T. DebRoy, H.L. Wei, J.S. Zuback, T. Mukherjee, J.W. Elmer, J.O. Milewski, A.M. Beese, A. Wilson-Heid, A. De, W. Zhang, Prog. Mater. Sci. 92 (2018) 112–224.
[13] T. Vilaro, V. Kottman-Rexerodt, M. Thomas, C. Colin, P. Bertrand, L. Thivillon, S. Abed, V. Ji, P. Aubry, P. Peyre, T. Malot, in: THERMEC 2009 Suppl., Trans Tech Publications, 2010, pp. 586–591.
[14] B. Zheng, Y. Zhou, J.E. Smugeresky, E.J. Lavernia, Metall. Mater. Trans. A 40 (2009) 1235–1245.
[15] S. Katakam, J.Y. Hwang, S. Paital, R. Banerjee, H. Vora, N.B. Dahotre, Metall. Mater. Trans. A 43 (2012) 4957–4966.
[16] K.G. Prashanth, H. Shakur Shahabi, H. Attar, V.C. Srivastava, N. Ellendt, V. Uhlenwinkel, J. Eckert, S. Scudino, Addit. Manuf. 6 (2015) 1–5.
[17] X. Lu, M. Nursulton, Y. Du, W. Liao, Materials 12 (2019) 775.
[18] S. Pauly, L. Löber, R. Petters, M. Stoica, S. Scudino, U. Kühn, J. Eckert, Mater. Today 16 (2013) 37–41.
[19] L. Deng, S. Wang, P. Wang, U. Kühn, S. Pauly, Mater. Lett. 212 (2018) 346–349.
[20] P. Zhang, C. Zhang, D. Ouyang, L. Liu, Scr. Mater. 192 (2021) 7–12.
[21] A. Ericsson, V. Pacheco, M. Sahlberg, J. Lindwall, H. Hallberg, M. Fisk, Mater. Des. 195 (2020) 108958.
[22] C. Yang, C. Zhang, W. Xing, L. Liu, Intermetallics 94 (2018) 22–28.
[23] D. Ouyang, N. Li, W. Xing, J. Zhang, L. Liu, Intermetallics 90 (2017) 128–134.
[24] N. Sohrabi, J. Jhabvala, G. Kurtuldu, R. Frison, A. Parrilli, M. Stoica, A. Neels, J.F. Löffler, R.E. Logé, Appl. Mater. Today (2021) Submitted for publication.
[25] S. Liu, A. Dhiman, Y.C. Shin, V. Tomar, S.T. Zhang, Intermetallics 111 (2019) 106503.
[26] J.E.K. Schawe, S. Pogatscher, in: C. Schick, V. Mathot (Eds.), Fast Scanning Calorimitry, Springer International Publishing, Cham, 2016, pp. 3–80, doi:10.1007/978-3-319-31329-0_1.
[27] J. Orava, A.L. Greer, B. Gholipour, D.W. Hewak, C.E. Smith, Nat. Mater. 11 (2012) 279–283.
[28] S. Pogatscher, D. Leutenegger, A. Hagmann, P.J. Uggowitzer, J.F. Löffler, Thermochim. Acta 590 (2014) 84–90.
[29] S. Pogatscher, P.J. Uggowitzer, J.F. Löffler, Appl. Phys. Lett. 104 (2014) 251908.
[30] J.Q. Wang, Y. Shen, J.H. Perepezko, M.D. Ediger, Acta Mater 104 (2016) 25–32.
[31] F.X. Bai, J.H. Yao, Y.X. Wang, J. Pan, Y. Li, Scr. Mater. 132 (2017) 58–62.
[32] F. Haag, S. Geisel, G. Kurtuldu, J.F. Löffler, Acta Mater 151 (2018) 416–423.
[33] Q. Cheng, X. Han, I. Kaban, I. Soldatov, W.H. Wang, Y.H. Sun, J. Orava, Scr. Mater. 183 (2020) 61–65.
[34] Y.P. Ivanov, C.M. Meylan, N.T. Panagiotopoulos, K. Georgarakis, A.L. Greer, Acta Mater. 196 (2020) 52–60.
[35] P. Bordeenithikasem, M. Stolpe, A. Elsen, D.C. Hofmann, Addit. Manuf. 21 (2018) 312–317.
[36] B. Bochtler, M. Stolpe, B. Reiplinger, R. Busch, Mater. Des. 140 (2018) 188–195.
[37] P. Drescher, K. Witte, B. Yang, R. Steuer, O. Kessler, E. Burkel, C. Schick, H. Seitz, J. Alloys Compd. 667 (2016) 109–114.
[38] J.E.K. Schawe, K.-U. Hess, Thermochim. Acta 677 (2019) 85–90.
[39] S. Pogatscher, D. Leutenegger, J.E.K. Schawe, P.J. Uggowitzer, J.F. Löffler, Nat. Commun. 7 (2016) 11113.
[40] J.E.K. Schawe, J.F. Löffler, Nat. Commun. 10 (2019) 1337.
[41] G.W.H. Höhne, H.K. Cammenga, W. Eysel, E. Gmelin, W. Hemminger, Thermochim. Acta 160 (1990) 1–12.
[42] J.E.K. Schawe, Thermochim. Acta 698 (2021) 178879.
[43] J.E.K. Schawe, Thermochim. Acta 603 (2015) 128–134.
[44] M.J. Richardson, N.G. Savill, Polymer 16 (1975) 753–757.
[45] C.T. Moynihan, A.J. Easteal, M.A.N.N. De Bolt, J. Tucker, J. Am. Ceram. Soc. 59 (1976) 12–16.
[46] J.E.K. Schawe, J. Chem. Phys. 141 (2014) 184905.
[47] J.E.K. Schawe, Thermochim. Acta 461 (2007) 145–152.
[48] I.S. Gutzow, J.W.P. Schmelzer, The Vitreous State - Thermodynamics, Structure, Rheology, and Crystallization, 2nd Ed, Springer-Verlag, Berlin, 2013.
[49] D.V Louzguine-Luzgin, A. Inoue, Phys. B Condens. Matter 358 (2005) 174–180.